

The British University in Egypt

BUE Scholar

Pharmacy

Health Sciences

Fall 1-25-2023

Development of potent nanosized carbonic anhydrase inhibitor for targeted therapy of hypoxic solid tumors

Ekram Hany Mohamed

The British University in Egypt, ekram.hany@bue.edu.eg

Wagdy M. Eldehna,

Department of Pharmaceutical Chemistry, Faculty of Pharmacy, Kafrelsheikh University, Kafrelsheikh, 33516, Egypt

Mahmoud A. El Hassab

Department of Pharmaceutical Chemistry, Faculty of Pharmacy, King Salman International University (KSIU), South Sinai, Egypt

Nahla A. Abdelshafi,

Department of Pharmaceutical Analytical Chemistry, School of Pharmacy, Badr University in Cairo, Cairo, Badr City, 11829, Egypt

Follow this and additional works at: <https://buescholar.bue.edu.eg/pharmacy>



Part of the [Analytical, Diagnostic and Therapeutic Techniques and Equipment Commons](#)

Recommended Citation

Mohamed, Ekram Hany; Eldehna,, Wagdy M.; El Hassab, Mahmoud A.; and Abdelshafi,, Nahla A., "Development of potent nanosized carbonic anhydrase inhibitor for targeted therapy of hypoxic solid tumors" (2023). *Pharmacy*. 676.

<https://buescholar.bue.edu.eg/pharmacy/676>

This Research Project is brought to you for free and open access by the Health Sciences at BUE Scholar. It has been accepted for inclusion in Pharmacy by an authorized administrator of BUE Scholar. For more information, please contact bue.scholar@gmail.com.



Development of potent nanosized carbonic anhydrase inhibitor for targeted therapy of hypoxic solid tumors

Wagdy M. Eldehna^{a,b,*}, Mahmoud A. El Hassab^c, Nahla A. Abdelshafi^d, Rana A. Eissa^b, Nadeen H. Diab^{b,m}, Ekram H. Mohamed^e, Mamdouh A. Oraby^f, Sara T. Al-Rashood^g, Rana G. Eissa^h, Zainab M. Elsayedⁱ, Alessio Nocentini^j, Claudiu T. Supuran^j, Mahmoud Elsabahy^{b,k,*}, Noura G. Eissa^{b,l}

^a Department of Pharmaceutical Chemistry, Faculty of Pharmacy, Kafrelsheikh University, Kafrelsheikh 33516, Egypt

^b School of Biotechnology and Science Academy, Badr University in Cairo, Badr City, Cairo 11829, Egypt

^c Department of Pharmaceutical Chemistry, Faculty of Pharmacy, King Salman International University (KSIU), South Sinai, Egypt

^d Department of Pharmaceutical Analytical Chemistry, School of Pharmacy, Badr University in Cairo, Badr City, Cairo 11829, Egypt

^e Pharmaceutical Chemistry Department, Faculty of Pharmacy, The British University in Egypt, El Sherouk City, Cairo 11837, Egypt

^f Pharmacology Department, Faculty of Pharmacy, Badr University in Cairo, Cairo, Egypt

^g Department of Pharmaceutical Chemistry, College of Pharmacy, King Saud University, P.O. Box 2457, Riyadh 11451, Saudi Arabia

^h Biochemistry Department, Faculty of Pharmacy, Zagazig University, Zagazig 44519, Egypt

ⁱ Scientific research and innovation support unit, Faculty of Pharmacy, Kafrelsheikh University, Kafrelsheikh 33516, Egypt

^j Department of NEUROFARBA, Section of Pharmaceutical and Nutraceutical Sciences, University of Florence, Polo Scientifico, Via U. Schiff 6, 50019, Sesto Fiorentino, Firenze, Italy

^k Department of Chemistry, Texas A&M University, College Station, TX 77842, USA

^l Department of Pharmaceutics, Faculty of Pharmacy, Zagazig University, Zagazig 44519, Egypt

^m Pharmaceutics Department, Faculty of Pharmacy, Sphinx University, New Assiut City, Assiut, Egypt

ARTICLE INFO

Keywords:

Hypoxic solid tumors
Hypoxia
Niosomes
Carbonic anhydrase
Nanoparticles
HIF-1 α
MMP-2
VEGF

ABSTRACT

Overexpression of two carbonic anhydrase (CA) isoforms, CA IX and XII, in several hypoxic solid tumors provides an extracellular hypoxic microenvironment, interferes with extra- and intracellular pH regulation, thus favoring hypoxic tumor cell survival, proliferation and metastasis. In the current study, a selective inhibitor for human CA isoforms IX and XII (isatin-bearing sulfonamide, WEG-104), was incorporated into nanosized spherical niosomes at high encapsulation efficiency to allow for an enhanced and sustained antitumor activity. *In vivo*, administration of WEG-104 that is either free (10 mg/kg) or loaded into niosomes (5 mg/kg) into a mice model of Ehrlich ascites solid tumor resulted in comparable efficacy in terms of reduction of tumor weight and volume. Administration of WEG-104-loaded niosomes (10 mg/kg) exhibited superior antitumor activity compared to the free drug, evidenced by reduced tumor weight and volume, marked reduction in the activity of CA IX and XII, and suppression of HIF-1 α and MMP-2. Moreover, prominent increase of caspase 3 and pronounced decrease in VEGF immune expression were observed in the treated animals. Hence, loading of molecularly designed compounds that targets CAs in hypoxic solid tumors into nanosized delivery systems provided an auspicious strategy for limiting solid tumor progression and malignancy.

1. Introduction

Cancer is a leading cause of death worldwide with a dramatically increasing prevalence. According to the GLOBOCAN statistics published by the International Agency for Research on Cancer, 18.1 million new cases and 9.8 million cancer deaths were estimated in 2018 (Bray et al.,

2018). Hypoxia, a common feature of solid tumors, renders tumors more resistant to conventional therapeutic treatments including chemotherapy, radiotherapy, and photodynamic therapy (Liu et al., 2018). The hypoxic tumor microenvironment allows for a rapid tumor progression, enhances the malignancy of several tumor cell lines, and consequently lowers survival rates in patients.

* Corresponding authors.

E-mail addresses: wagdy2000@gmail.com (W.M. Eldehna), mahmoud.elsabahy@chem.tamu.edu (M. Elsabahy).

<https://doi.org/10.1016/j.ijpharm.2022.122537>

Received 14 August 2022; Received in revised form 19 December 2022; Accepted 20 December 2022

Available online 23 December 2022

0378-5173/© 2022 Elsevier B.V. All rights reserved.

Carbonic anhydrases (CAs) expressed in humans are metalloenzymes (*i.e.*, zinc (II)-dependent) involved in vital physiological processes (*e.g.*, maintaining acid-base homeostasis, pH regulation and fluid balance) (Supuran, 2008). Abnormalities in the expression of CAs may lead to diseases (*e.g.*, hypertension, glaucoma, epilepsy, cancers, pH disequilibria, *etc.*). CA IX and XII isoforms are two out of fifteen human isoforms of CAs that are overexpressed in many hypoxic solid tumors (*e.g.*, colon, breast, renal, lung, ovarian carcinomas, *etc.*) due to activation of the hypoxia inducible factor (HIF) cascade. CA IX and XII show limited expression in normal tissues (Supuran, 2020). These enzymes are involved in extra- and intra-cellular pH regulation to provide an extra-cellular acidic, hypoxic microenvironment suitable for the hypoxic tumor cell survival and proliferation. Thus, CA IX and XII were considered as targets for management of hypoxic solid tumors, and several CA inhibitors (*e.g.*, SLC-0111) are undergoing preclinical and clinical investigations as antitumor agents (Vats et al., 2019).

Molecular design and synthesis of selective inhibitors of human CA isoforms is considered a promising approach for management of hypoxic solid tumors while minimizing side effects of the currently used therapeutic agents. Recently, isatin has been arising as a promising tail scaffold for the design of compounds possessing CA inhibitory activities, including anticancer activity (Li et al., 2018). Since the FDA approval of two isatin-based anticancer drugs, namely, Nintedanib (Ofev®) and Sunitinib (Sutent®) (Goodman et al., 2007; McCormack, 2015), extensive research efforts were performed by our group (Abdel-Aziz et al., 2017; Eldehna et al., 2018, 2017) and others (Gao et al., 2017; Ibrahim et al., 2015) towards the development of isatin-based compounds as anticancer agents. In this context, our group has synthesized isatin-bearing sulfonamides with preferential inhibitory activity against CA IX and XII over the cystolic off-target isoforms (*e.g.*, CA I and II) (Eldehna et al., 2018).

Nanovesicular drug delivery systems comprised of non-ionic amphiphilic surfactants together with cholesterol (*i.e.* niosomes) (Thabet et al., 2021), have been widely utilized for several biomedical applications (Allam et al., 2021, 2019; Aparajay and Dev, 2022; Eldehna et al., 2022; Li et al., 2022) owing to their ability to encapsulate both hydrophilic and lipophilic cargoes, and their unique characteristics (*e.g.*, low toxicity, high stability, low manufacturing cost, ease of formulation and scale-up) (Ge et al., 2019; Thabet et al., 2021). Synthesis of new therapeutic compounds and their incorporation into nanovesicular structures provides a promising strategy for enhancing stability and therapeutic activity of these molecules (Eldehna et al., 2022). In the current study, *in silico* molecular docking studies were performed, and an isatin-bearing sulfonamide (WEG-104) was synthesized and incorporated into a nanoparticulate delivery system, niosomes, to allow for an enhanced antitumor activity. Several *in vitro* and *in vivo* characterizations have been carried out to assess the ability of niosomes to encapsulate the newly synthesized compound and to evaluate their antitumor activities in a hypoxic solid tumor model.

2. Materials and methods

2.1. Materials

WEG-104 is a synthesized CA IX and XII isoforms inhibitor (Eldehna et al., 2018). Polyoxyethylene sorbitan monopalmitate (Tween® 40), sorbitan monostearate (Span® 60) and cholesterol were purchased from Sigma-Aldrich (St. Louis, MO, USA). Chloroform (HPLC grade) was purchased from El-Nasr Pharmaceutical Co. (Cairo, Egypt). Disodium hydrogen phosphate and potassium dihydrogen phosphate were purchased from Adwic, El-Nasr Chemical Co. (Cairo, Egypt). Dialysis tubing membrane, molecular weight cut-off 12,000–14,000, was purchased from Carolina Biological Supply Co. (Burlington, NC, USA).

2.2. Synthesis of 4-(2-((1-benzyl-5-chloro-2-oxoindolin-3-ylidene)amino)ethyl) benzenesulfonamide (WEG-104)

An amount (0.135 g, 0.5 mmol) of 1-benzyl-5-chloroisatin **2** was dissolved in 5 mL boiling ethanol and catalytic drops of glacial acetic acid. Then, the required amount (0.1 g, 0.5 mmol) of 4-(2-aminoethyl) benzenesulfonamide **3** was added to the reaction mixture. Reflux was continued for 2 h, and then the precipitated solid was filtered off while hot, washed with cold methanol (2 × 3 mL), dried and recrystallized from isopropanol to yield WEG-104; yellow powder (0.17 g, 76 % yield); MP above 280 °C (Eldehna et al., 2017).

2.3. Molecular docking study

The free access Vina Autodock software was implemented to conduct the entire docking study (Trott and Olson, 2010). The crystal structures of CA XII and CA IX were downloaded from the protein data bank using the following PDB IDs: 6YH9 and 6UGZ, respectively. WEG-104 was drawn using Chemdraw and converted to 3D structure by Biovia discovery visualizer (<https://3dsbiovia.com/resource-center/download-s/>). As Vina Autodock requires the receptor and the ligands in pdbqt format, M.G.L tools were utilized. In addition, the active sites were determined via the construction of grid box surrounding the binding of the co-crystallized ligands. Finally, WEG-104 was docked into the pre-determined active sites of CA XII and CA IX enzymes. The docking results were visualized by Biovia discovery studio 2020 free visualizer (<https://3dsbiovia.com/resource-center/downloads/>) that was used to generate 2D and 3D interactions for the docked poses.

2.4. Preparation of niosomes

WEG-104-loaded niosomes were prepared via thin-film hydration technique, as previously reported (Thabet et al., 2021). Precisely weighed amounts of cholesterol, Span® 60 and Tween® 40 (molar ratio of 2:1:1, respectively) were added to 15 mL mixture of chloroform and ethanol (1:2 v/v, respectively) in which the drug was initially dissolved. The organic solvent was then evaporated under reduced pressure using a rotary evaporator (Buch 200, BÜCHI Labortechnik AG, Flawil, Switzerland) at 40 °C at 110 rpm for 30 min to form a thin-lipid film. The resultant dried thin lipid film was hydrated with 10 mL of distilled water under gentle shaking for 60 min at 60 °C to allow for the formation of drug-loaded niosomal dispersion. The samples were sonicated by a probe sonicator (Branson Digital Sonifier SFX 250, St. Louis, MO) for 1 min (50 Hz, while turning the sonicator off and on every 2 s) to obtain niosomes of homogenous size distribution. The samples were then centrifuged at 13,400 rpm for 30 min to produce niosomal pellets. The pellets were then washed with distilled water, and final pellets were diluted with distilled water and vortexed to form the niosomal dispersion.

2.5. Characterizations of niosomes

2.5.1. Dynamic light scattering and evaluation of entrapment efficiency

Dynamic light scattering measurements and evaluation of entrapment efficiency were performed as described earlier (Supplementary Materials, S1) (Saafan et al., 2021).

2.5.2. Transmission electron microscopy

The morphology of the dispersed particles was studied using the transmission electron microscopy (JEM-2100 Plus, Electron Microscope, JEOL, Japan) (Supplementary Materials, S2).

2.5.3. Fourier transform-infrared spectroscopy

Characteristic peaks of WEG-104, drug-loaded niosomes and empty niosomes were recorded using the Fourier transform-infrared spectrophotometer (FTIR-8400s Shimadzu, Japan). From each sample, 10 mg

powder was mixed with potassium bromide (spectroscopic grade) prior to compression into discs using hydraulic press. Samples were then scanned from 4000 to 400 cm^{-1} .

2.6. In vitro release study

In vitro release study of WEG-104 from freshly prepared niosomes was performed using the dialysis method as previously reported (**Supplementary Materials, S3**) (Saafan et al., 2021).

2.7. Anti-proliferative activity of WEG-104 and WEG-104-loaded niosomes

The anti-proliferative activity of WEG-104 and WEG-104-loaded niosomes were screened against breast cancer cell line (MCF-7, ATCC) utilizing MTT assay, as reported previously (**Supplementary Materials, S4**) (Eldehna et al., 2021; Mosmann, 1983).

2.8. In vivo evaluation of the developed nanomaterials

Adult female mice of Swiss albino strain weighing 15–20 g were used in the present study. Animals were obtained from the Animal House of Faculty of Pharmacy, Badr University in Cairo (Cairo, Egypt). Mice were housed in polypropylene cages under controlled laboratory conditions (23 ± 1 °C, 40–60 % humidity), with alternating cycles of 12 h light/dark. Mice were fed standard mice pellet diet, had water *ad libitum*, and maintained for an acclimation period of one week before the experiment. The experimental procedures were approved by the Research Ethics Committee of the Faculty of Pharmacy, Badr University in Cairo (PO-104-A) and complied with the guidelines of the US National Institutes of Health for the proper care and use of laboratory animals (NIH Publication No. 85–23, revised 1996).

According to the method described by Lorke (Lorke, 1983), lethal dose that kills 50 % of the tested animals (LD_{50}) was determined in two steps including a total of 13 male rats (weighing 150–200 gm), which were obtained from the Animal House of Faculty of Pharmacy, Badr University in Cairo. Rats were fasted for 18 h before the experiment. The first step involved 9 rats divided into 3 groups (3 rats each) which received 3 increasing doses of WEG-104 (10, 100 and 1000 mg/kg, intraperitoneal (i.p.), respectively). Rats were then observed for 24 h to observe any behavioral changes and to estimate mortality. Based on the results from the first step, the second step involved other 4 rats allocated into 4 groups (one rat each) and received 4 subsequent doses of WEG-104 (200, 400, 800 and 1600 mg/kg, i.p.). Animals were then observed for 24 h to monitor their behavior as well as mortality. Based on the results of the second step, LD_{50} was determined according to equation (1):

$$\text{LD}_{50} = \sqrt{D_0 \times D_{100}} \quad (1)$$

Where, D_0 = highest dose that did not cause mortality, and D_{100} = lowest dose that resulted in mortality.

Data are presented as means \pm SD and statistically analyzed by Graphpad prism software version 6 (San Diego, CA, USA) using one-way ANOVA followed by Tukey's multiple comparison tests. Change in tumor volume (TV) measured over time for each group was analyzed using a two-way ANOVA, followed by Tukey's multiple comparison tests. Differences between different groups were considered significant for p values < 0.05 .

2.8.1. Induction of Ehrlich ascites solid tumors

Mouse-bearing Ehrlich ascites carcinoma (EAC) was purchased from the National Cancer Institute (NCI), Cairo University (Cairo, Egypt). Tumor cells were maintained by intraperitoneal inoculation of ascitic fluid from EAC mice into normal mice every 10 d. Ascitic tumor cells were drawn from EAC mice at the log phase (7–8 d of tumor growth),

suspended, and diluted with PBS. Tumor suspension containing about 2×10^6 tumor cells (*ca.* 0.2 mL) was then transplanted subcutaneously into the tested groups (Aziz et al., 2016). Five days later, mice developed solid tumors as demonstrated by formation of palpable mass (50–100 mm^3).

Ehrlich ascites carcinoma mice were allocated into 5 groups (6 mice each) as follows: untreated EAC control group that received DMSO (10 mL/kg/d, *i.p.*) and treated EAC groups that received free WEG-104 (5 mg/kg/d, *i.p.*), free WEG-104 (10 mg/kg/d, *i.p.*), WEG-104-loaded niosomes (5 mg/kg/d, *i.p.*), and WEG-104-loaded niosomes (10 mg/kg/d, *i.p.*). Free-WEG-104 was dissolved in 5 % DMSO, and all treatments were given to EAC mice at the fifth day after subcutaneous implantation of tumor cells over 20 days. First day of treatment was considered as day 0.

2.8.2. Tumor volume (TV) and tumor growth inhibition (TGI)

The alteration in TV was estimated every 5 days from the first day of treatment (day 0) till the 20th day. The tumor diameter in each mouse was measured using a digital vernier caliper and TV was calculated using the following equation:

$$\text{TV} = \text{length (mm)} \times [\text{width (mm)}]^2 \times 0.52 \quad (2)$$

TGI for each group was monitored as follows:

$$\text{TGI (\%)} = 1 - (\text{RTV of each treated group} / \text{RTV of the control or untreated group}) \times 100 \quad (3)$$

where RTV is the relative tumor volume of each group = (TV measured at day 20 / TV measured at day 0).

Following 20 days of treatment, blood samples were collected from the retro-orbital plexus using microcapillary tubes, and serum was separated via centrifugation at 4500 rpm for 20 min. Serum samples were stored at -20 °C to further analyze the concentration of WEG-104 in the different treatment groups using ultra performance liquid chromatography (UPLC). Separation was performed on hypersil column (C_{18}). The optimized mobile phase comprised of methanol: water (70:30 v/v). The flow rate was adjusted at 0.4 mL/min, and the injection volume used was 20 μL , and the drug was detected at a wavelength of 260 nm.

Mice serum samples were thawed at room temperature and vortexed for one minute. Then, 150 μL of acetonitrile was added to 50 μL of serum sample, followed by centrifugation for 15 min at 15,000 rpm for protein precipitation. Drug free serum was spiked with WEG-104, followed by sample preparation, as mentioned earlier. Measurement of the drug concentration was carried out, and recovery percentage was evaluated. Seven standard stock solutions of the free drug (WEG-104) in the range of 1–50 $\mu\text{g/mL}$ in PBS buffer were prepared for construction of the calibration curve for WEG-104. A volume of 20 μL of each standard was injected in triplicate and the chromatographic signal was obtained using the aforementioned chromatographic conditions. Linear plot was obtained by plotting peak area against standard concentration.

Analytical method validation was performed according to ICH guidelines. Peak areas of seven standard solutions with 1, 5, 10, 20, 30, 40, 50 $\mu\text{g/mL}$ concentrations were plotted against concentrations for constructing the calibration curve. ICH parameters such as linearity, range, and % RSD were measured three times. Accuracy of the chromatographic method was calculated as percent recovery from analyzing three different concentrations (15, 25 and 45 $\mu\text{g/mL}$), and mean \pm % RSD of three concentrations of the drug was estimated. Precision (inter-day precision) was evaluated by measuring three concentrations (10, 30 and 50 $\mu\text{g/mL}$) at three different days. Repeatability (intra-day precision) was evaluated by analyzing three different concentrations in triplicates (10, 30 and 50 $\mu\text{g/mL}$). Robustness of the developed method was assessed by analyzing drug concentrations upon changes in the experimental conditions. Changing the mobile phase composition (± 5 mL), flow rate (± 0.05 mL/min), pH of buffer (± 0.2), and column

temperature (± 2 °C) did not show any significant effect on peak signal and its resolution. Limit of detection (LOD) and limit of quantification (LOQ) were estimated using signal to noise ratio, 3.3:1 (LOD) and 10:1 (LOQ). Free drug concentrations of 20 and 50 $\mu\text{g}/\text{mL}$ were spiked in mice serum, protein precipitation was performed as mentioned earlier, and recovery percentage was assessed.

Mice were then sacrificed by cervical dislocation and tumor masses were excised, washed with ice-cold saline, dried, and weighed. A part of tumor specimens for each mouse was fixed in 10 % formalin for histopathological and immunohistochemistry examinations. The remaining tumor tissues were weighed and rapidly frozen in liquid nitrogen and stored at -80 °C for biochemical studies and protein analyses.

2.8.3. Biological estimation of carbonic anhydrases IX, XII (CA IX & CA XII) and hypoxia-inducible factor-1 α (HIF-1 α), matrix metalloproteinases-2 (MMP-2), and caspase-3 in tumor tissues of EAC mice

Commercially available enzyme-linked immunosorbent assay (ELISA) kits were used for estimation of the activity of CA IX (Cat#: NBP2-71283; Novus Biologicals, USA) and CA XII (Cat#: abx556084; Abnova Ltd, Cambridge, UK) as well as the protein content of HIF-1 α (Cat#: orb397111; Biorbyt Ltd, UK), MMP-2 (Cat#: E-EL-M0780; Elabscience, USA), and caspase-3 (Cat#: E4591-100; BioVision, USA) according to the instructions provided by the manufacturers.

2.8.4. Histopathological examination

Specimens of EAC tissues were immersed and fixed in 10 % neutral-buffered formalin. Serial grades of ethanol were used for dehydration of tumor tissues which were afterward cleared in xylene and embedded in paraffin wax. About 4- μm thickness of embedded tumor sections were used for staining by hematoxylin & eosin (H & E) and examined under light microscope (magnification of 400 \times).

2.8.5. Immunohistochemistry - analysis of VEGF

Paraffin embedded tumor sections were dewaxed for immunohistochemical analysis according to the manufacturer's instruction. Deparaffinized retrieved tumor tissues were treated with 0.3 % H_2O_2 for 20 min followed by incubation with anti-VEGF mouse monoclonal antibody (Cat#: GB14165; 1:200; Servicebio, China) at 4 °C overnight. Sections were then washed out by PBS and incubated with secondary antibody (HRP Envision kit; DAKO) for 20 min followed by incubation with diaminobenzidine for 15 min. Specimens were washed with PBS and counterstained with Mayer's hematoxylin (Sigma-Aldrich, Inc., St. Louis, MO, USA) for microscopic examination. For determination of VEGF immunoreactive area (%) in tumor tissues, 6 non-overlapping fields (mean \pm SD of 6 fields) were randomly selected. Images of stained tumor slides were analyzed using full HD microscopic imaging system linked to Leica application suite (Leica Microsystems GmbH, Germany).

2.8.6. Prediction of pharmacokinetic parameters and potential toxicity

Two freely available online servers namely (preadmet: <https://preadmet.webservice.bmdrc.org/adme/> and fu,p Predictor: <https://adm.e.nibiohn.go.jp/fup>) were employed to predict the pharmacokinetic profile of the compound WEG-104. On the other hand, the Toxpred

online server was utilized to evaluate potential toxicity of WEG-104.

3. Results and discussion

3.1. Preparation of (WEG-104)

The organic synthesis of **WEG-104** was carried out as depicted in **Scheme 1**. In the first step, the 5-chloroisatin (**1**) was benzylated via the reaction with benzyl bromide, in dimethylformamide as a solvent and anhydrous K_2CO_3 as a base, to produce the corresponding 1-benzyl-5-chloroisatin (**2**). Thereafter, *N*-benzyl derivative (**2**) was condensed with 4-(2-aminoethyl)benzenesulfonamide (**3**) in absolute ethanol and glacial acetic acid mixture to afford the formation of the target carbonic anhydrase inhibitor **WEG-104** (**Scheme 1**). Physical properties, spectral data (IR and ^1H NMR), elemental analysis, and purity for **WEG-104** were provided in the **Supplementary Materials (S5)**.

3.2. In vitro carbonic anhydrase inhibitory activity

The CA inhibitory activity of **WEG-104** was *in vitro* evaluated previously (**Eldehna et al., 2018, 2017**) against a panel of hCA isoforms (hCA I, II, IV and VII), as well as, against the cancer-associated hCA IX and XII isoforms. The inhibition constant (K_i) for each isoform is presented in **Table 1**.

The results disclosed that **WEG-104** weakly affected the off-target isoforms (hCA I, II, IV and VII), whereas, it effectively inhibited both cancer-associated hCA IX and XII isoforms with $K_{iS} = 10.5$ and 32.7 nM, respectively (**Table 1**).

Furthermore, selectivity ratio for the inhibition of hCA IX and XII over hCA I, II, IV, and VII for **WEG-104** was calculated and listed in **Table 2**.

3.3. Molecular docking study

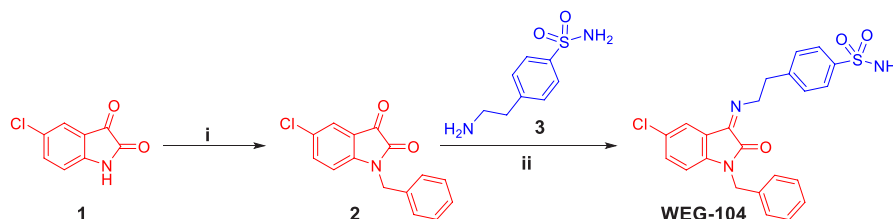
This section was conducted to elucidate the potential binding mode of **WEG-104** with CA XII and CA IX enzymes. As reported previously, the sulfonamide group allowed the necessary hydrophilic interactions with both the CA XII and CA IX enzymes. The hydrophobic interactions were achieved through the lipophilic chloroisatin and phenyl rings. As can be seen in **Fig. 1**, **WEG-104** was able to produce multiple interactions upon binding with CA XII, where the sulfonamide group formed two hydrogen bonds with Thr199 and Thr200, while ionic and metal coordinate bonds

Table 1

Inhibition data of hCA isoforms hCA I, II, IV, VII, IX and XII with **WEG-104** determined by stopped-flow CO_2 hydrase assay, using acetazolamide (AAZ) as a standard drug.

Compound	K_i (nM) ^a					
	hCA I	hCA II	hCA IV	hCA VII	hCA IX	hCA XII
WEG-104	8550.9	713.9	1799.5	> 10000	10.5	32.7
AAZ	250	12	74	2.5	25	5.7

^a Mean from 3 different assays, by a stopped flow technique (**Eldehna et al., 2018, 2017**).



Scheme 1. Synthesis of **WEG-104**; Reagents and conditions: (i) Benzyl bromide, dimethylformamide, potassium carbonate, reflux 3 h; (ii) Absolute ethanol, glacial acetic acid, reflux 2 h.

Table 2

Selectivity ratio for the inhibition of hCA IX and XII over hCA I, II, IV and VII for WEG-104 and acetazolamide.

Compound	Selectivity ratio							
	I/ IX	II/ IX	IV/ IX	VII/ IX	I/ XII	II/ XII	IV/ XII	VII/ XII
WEG-104	814	68	171	> 952	261	22	55	306
AAZ	10	0.5	3	0.1	44	2	13	0.4

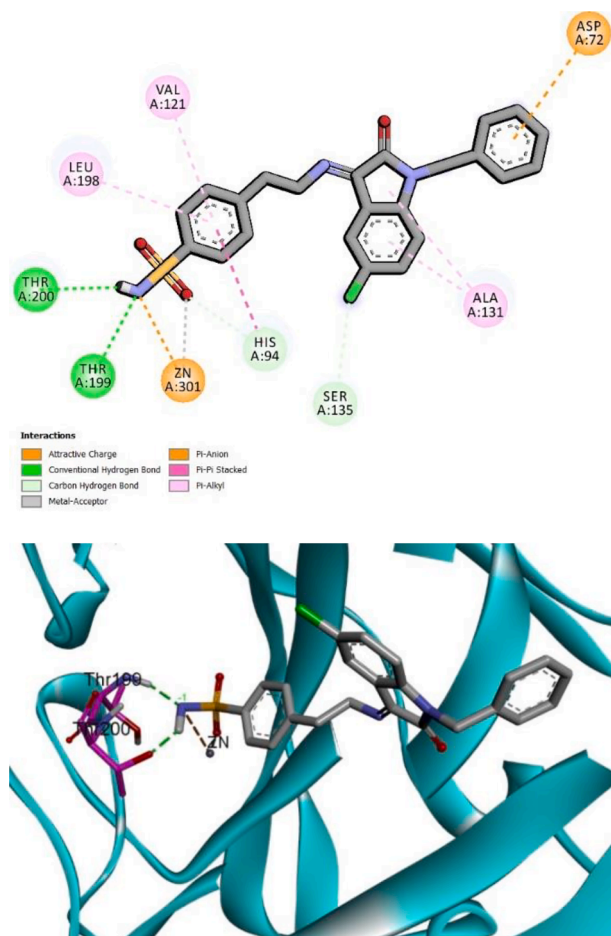


Fig. 1. Two- and three-dimensional diagrams for interactions of WEG-104 with CA XII.

were formed with the key Zinc ion involving coordination of the sulfonamide anion to the metal through the nitrogen atom. Moreover, the phenyl ring attached to the sulfonamide group formed multiple hydrophobic interactions with His94, Val121 and Leu198. Furthermore, the chlorisatin moiety interacted with Ala131 and Ser135, while *N*-substituted benzyl ring interacted with Asp72. Similar to the previous findings, the sulfonamide group of WEG-104 extensively interacted with CA IX residues forming two hydrogen bonds with His94 and Thr199, as well as Pi-sulfur interactions with His94 and His96 and Trp209, besides an ionic bond with the key Zinc metal (Fig. 2).

The chlorisatin ring contributed to hydrophobic interaction with Val131 in addition to three interactions with three solvent molecules. The aliphatic carbon of the *N*-benzyl formed an interaction with Gln67. A worthy note, the strong binding mode of WEG-104 with CA XII and CA IX enzymes was evidenced by excellent docking scores of -13.7 and -14.1 Kcal/mole, respectively.

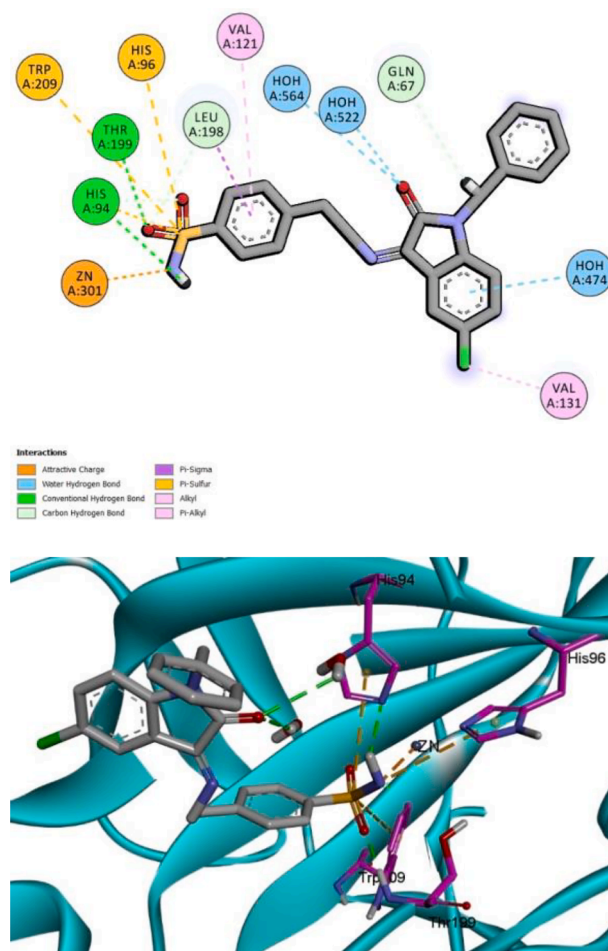


Fig. 2. Two- and three-dimensional diagrams for interactions of WEG-104 with CA IX.

3.4. Preparation and characterizations of WEG-104-niosomal dispersion

Niosomes comprised of cholesterol, Span® 60 and Tween® 40 at a molar ratio of 2:1:1, respectively, were developed via thin-film hydration technique, as previously reported by our group (Eldehna et al., 2022; Saafan et al., 2021; Thabet et al., 2021) and others (Kashef et al., 2020; Ramadan et al., 2020). WEG-104-loaded niosomes displayed nanosized particles of mean number-averaged hydrodynamic diameter 465.7 ± 16.3 nm (Fig. 3, left panel) and polydispersity index (PDI) of 0.66. WEG-104-loaded niosomes displayed negative zeta potential (i.e., -28.9 ± 0.8 mV), although surfactants used for the preparation of niosomes are nonionic themselves (i.e., Span® 60 and Tween® 40). Calibration curve of WEG-104 solution was established ($\lambda = 260$ nm, concentrations range of 12.5–100 $\mu\text{g/mL}$). The developed niosomes demonstrated high entrapment of WEG-104 (i.e., 93.0 ± 0.7 %). WEG-104-loaded niosomes displayed spherical morphology as illustrated by TEM (Fig. 3, right panel).

Fourier transform-infrared (FT-IR) spectroscopic analyses were performed to reveal any physical or chemical interactions between WEG-104 and the components of niosomes. FT-IR spectra of the non-ionic surfactants utilized for the preparation of the niosomes (i.e., Span® 60 and Tween® 40) and cholesterol have been previously reported by our group (Mohamed et al., 2017). FT-IR spectra of WEG-104, empty and WEG-104-loaded niosomes, are illustrated in Fig. 4. Spectrum of WEG-104 showed characteristic peaks at 3281.25 cm^{-1} which corresponds to N–H stretching, 1708.28 cm^{-1} which corresponds to C=O, 1608.39 cm^{-1} which corresponds to N–H bending, 1312.61 cm^{-1} and 560 cm^{-1} corresponding to S=O and C-Cl stretching, respectively. Similar spectra

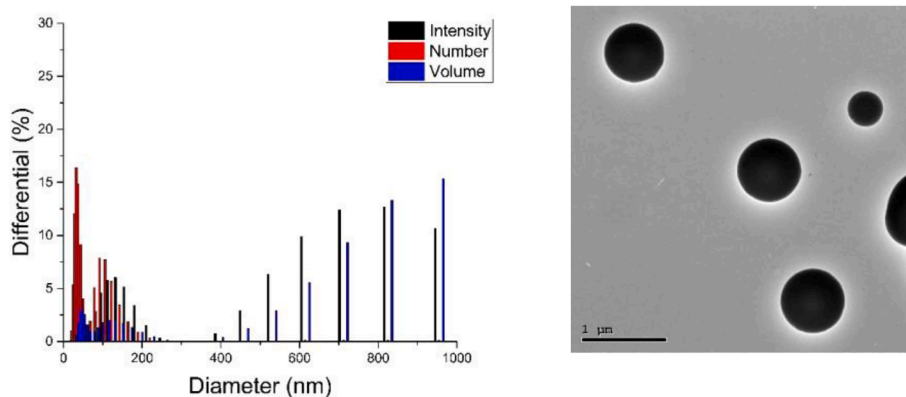


Fig. 3. Histograms of the intensity-, volume- and number-averaged hydrodynamic diameters of WEG-104-loaded niosomal dispersion (left panel). Transmission electron microscopy images of WEG-104-loaded niosomes (right panel). Scale bar represents 1 μm .

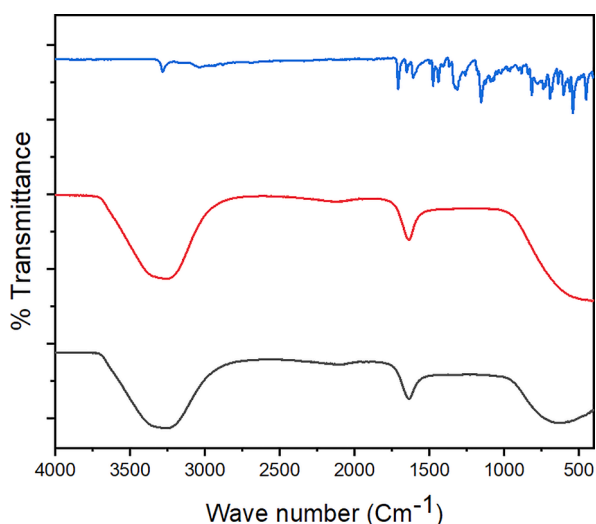


Fig. 4. Fourier transform-infrared spectra of WEG-104 (A), empty niosomes (B) and WEG-104-loaded niosomes (C).

were observed for empty and WEG-104-loaded niosomes, with the disappearance of the characteristic peaks of WEG-104 in the case of drug-loaded niosomes, indicating successful incorporation of the drug into the niosomes.

3.5. *In vitro* release studies

The mean cumulative drug release percentage of WEG-104, either free or loaded into niosomes, was measured and the amount of WEG-104 released over 48 h was calculated. Fig. 5 illustrates that incorporation of WEG-104 into niosomes resulted in a reduced initial burst release (*i.e.*, the percentage of WEG-104 released from the niosomes after 2 h was *ca.* 2.5-fold lower than that of the free drug). The encapsulation of the drug into the nanocarrier (*i.e.*, niosomes) allowed for an extended-release profile that was maintained all over the study.

3.6. Anti-proliferative activity of WEG-104 and WEG-104-loaded niosomes

To assess the anti-proliferative activity of WEG-104, free or loaded into niosomes, the cytotoxic activity against MCF-7 cell line was evaluated utilizing MTT assay, as compared to doxorubicin. WEG-104 and WEG-104-loaded niosomes displayed IC_{50} values of 5.17 and 6.04 μM , respectively, while doxorubicin demonstrated IC_{50} value of 2.37 μM .

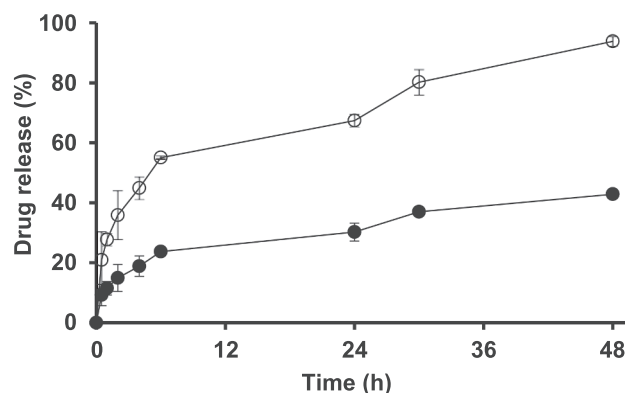


Fig. 5. *In vitro* release profiles of WEG-104, either free (open circle), or incorporated into niosomes (closed circle) over 48 h in PBS at pH 7.2 and 37 $^{\circ}\text{C}$.

3.7. *In vivo* evaluation

3.7.1. Acute toxicity study (LD_{50} of WEG-104)

Assessment of LD_{50} showed that two rats died at a dose of 1000 mg/kg, whereas no mortality was observed in groups received either 10 or 100 mg/kg of WEG-104. According to Lorke's method (Lorke, 1983), four increasing doses (200, 400, 800 and 1600 mg/kg, *i.p.*) were injected into four different groups (one rat each), respectively. Groups that received 200 mg/kg or 400 mg/kg (D_0 , highest dose with no mortality) survived, whereas groups that received 800 mg/kg (D_{100} , lowest dose causing mortality) or 1600 mg/kg died, indicating that WEG-104 has a high therapeutic index ($\text{LD}_{50} = 566$ mg/kg).

3.7.2. Effect of WEG-104 on tumor volume and weight in EAC mice

As depicted in Fig. 6 (upper panel), administration of free-WEG-104 at 5 mg/kg/d resulted in an evident decrease in the TV measured at d 15 and d 20 *versus* the corresponding untreated EAC mice with TGI of 39.0 %. However, administration of WEG-104-loaded niosomes at the same dose (*i.e.*, 5 mg/kg/d) exhibited a marked reduction in TV measured at d 10, 15 and 20 with TGI of 77.2 %. Intraperitoneal injection of free and WEG-104-loaded niosomes at 10 mg/kg/d induced a significant reduction of TV measured at d 5, 10, 15 and 20 as compared to the corresponding untreated EAC mice (TGI of 71.7 % and 87.0 %, respectively). Remarkably, a pronounced decline in TV was observed in WEG-104-loaded niosomes group compared to free-WEG-104 group using the same dose (5 mg/kg) at d 15 and 20 ($p = 0.0016$ and $p < 0.0001$, respectively). In addition, EAC mice treated with WEG-104-loaded niosomes displayed a marked decrease in TV relative to free-WEG-104 at a dose of 10 mg/kg/d at d 20 ($p = 0.0107$). Noticeably, TV of EAC

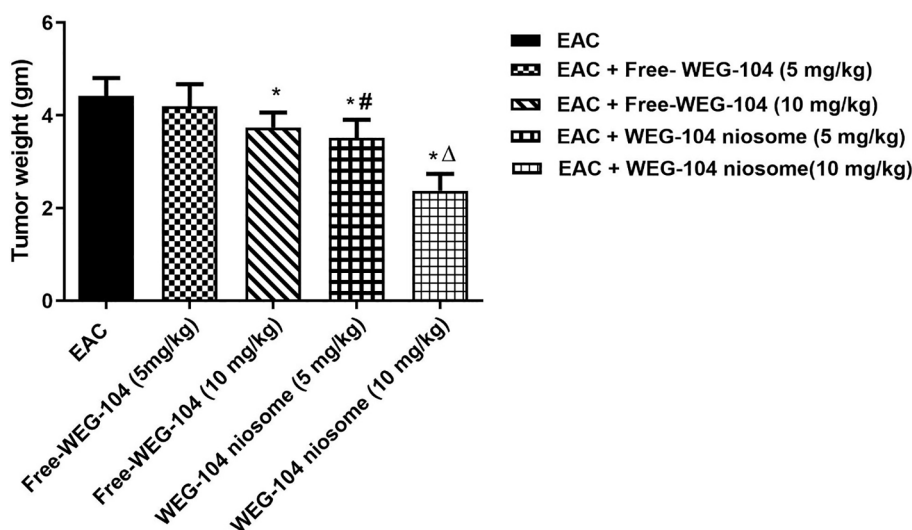
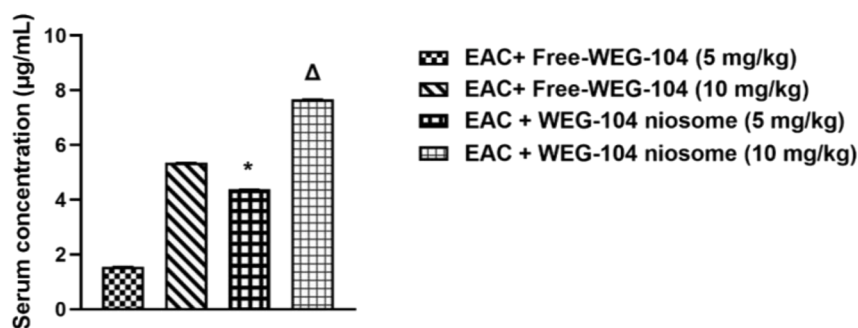
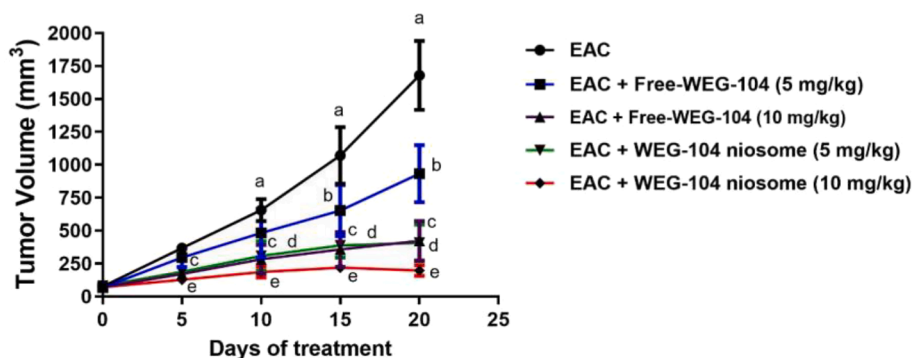


Fig. 7. Effect of WEG-104 on tumor weight of EAC mice. Free and WEG-104-loaded niosomes were intraperitoneally injected to EAC mice for 20 days using two doses (5 and 10 mg/kg/d). Data were represented as mean \pm S.D of 6 mice for each group. * versus untreated EAC, # versus free-WEG-104 (5 mg/kg/d). Δ versus free-WEG-104 (10 mg/kg/d).

mice that received free-WEG-104 at 10 mg/kg/d was comparable to that measured in mice received 5 mg/kg/d of WEG-104-loaded niosomes, particularly at d 10, 15 and 20 (TGI of 71.7 % and 77.2 %, respectively) (Fig. 6, upper panel).

To measure the serum concentration of WEG-104, a developed chromatographic method was performed and showed a recovery percentage of 99.58 ± 0.32 %. As shown in Figure S1 (Supplementary Material), the chromatogram of rat blank serum spiked with the drug illustrated a remarkable separation between the serum and drug peaks at different retention times of 0.60 and 1.37 min, respectively. Data

Fig. 6. Upper panel: Effect of WEG-104 on TV in EAC mice. Free- and WEG-104-loaded niosomes were intraperitoneally injected into EAC mice for 20 d using two doses (5 and 10 mg/kg/d). Tumor diameter of each mouse was calculated every 5 d from the first day of treatment (day 0) till day 20 using a digital vernier caliper. Data were represented as means \pm SD of 6 mice for each group, ^a Significant difference versus day 0 (control). b,c,d,e Significant difference of free-WEG-104 (5 mg/kg), free-WEG-104 (10 mg/kg), WEG-104-loaded niosomes (5 mg/kg), and WEG-104-loaded niosomes (10 mg/kg), respectively, versus the corresponding EAC. Lower panel: Serum concentration following intraperitoneal injection of free- and WEG-104-loaded niosomes into EAC mice for 20 d using two doses (5 and 10 mg/kg/d) on day 20 of the treatment. ^{*}, ^{Δ} Significant difference versus free-WEG-104 (5 mg/kg) and free-WEG-104 (10 mg/kg), respectively. EAC, Ehrlich ascites carcinoma.

obtained from the method validation showed a linearity range of 1–50 µg/mL with R^2 of 0.9999 (Figure S2, Supplementary Materials), a slope of $0.01036 \pm 1.75 \times 10^{-5}$ and intercept value of $8.58 \times 10^{-5} \pm 2.618 \times 10^{-4}$. The validation method resulted in an accuracy of 100.63 ± 1.58 and repeatability (intraday precision) of 2.053, precision of 2.238, limit of detection (LOD) of 0.08 µg/mL, and limit of quantification LOQ of 0.25 µg/mL. Fig. 6 (lower panel) illustrated a significant difference in the serum concentrations of free WEG-104 and WEG-104 niosomal dispersion, at both doses (i.e., 5 and 10 mg/kg).

Treatment of EAC mice with free-WEG-104 at 10 mg/kg/d and WEG-

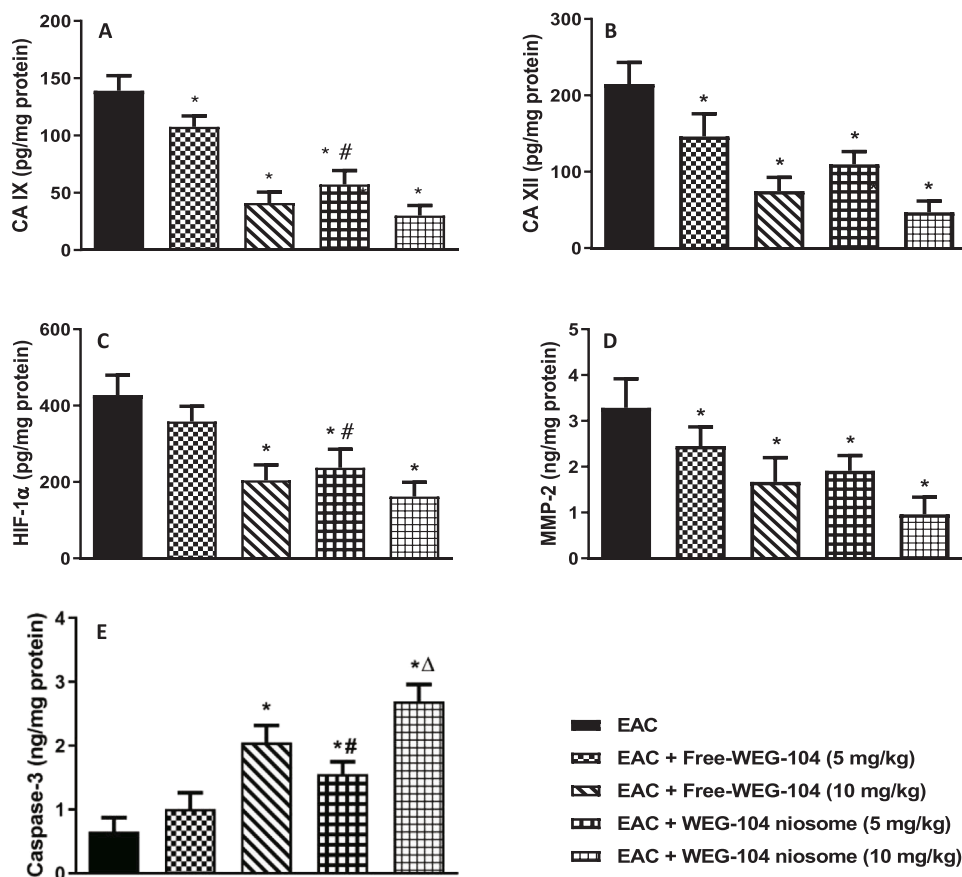


Fig. 8. Effect of WEG-104 on CA IX (A), CA XII (B), HIF-1 α (C), MMP-2 (D) and caspase-3 (E) of EAC mice. Free and WEG-104-loaded niosomes were intraperitoneally injected to EAC mice for 20 days using two doses (5 and 10 mg/kg/d). Data were represented as mean \pm S.D of 6 mice for each group. * versus untreated EAC, # versus free-WEG-104 (5 mg/kg/d), Δ versus free-WEG-104 (10 mg/kg/d).

104-loaded niosomes at 5 and 10 mg/kg/d for 20 d resulted in an apparent decrease in tumor weight by 15.5 %, 20.5 % and 46 % as compared to the untreated ones (Fig. 7). Strikingly, EAC mice that received either 5 or 10 mg/kg/d of WEG-104-loaded niosomes showed significant reduction in tumor weight in comparison to the mice that received free-WEG-104 at the same doses by ca. 16 % and 36.5 %, respectively ($p < 0.0001$).

3.7.3. Effect of WEG-104 on the activity of CA IX and CA XII

Administration of free- and WEG-104-loaded niosomes at the two doses (5 and 10 mg/kg/d) for 20 days resulted in a marked reduction in the activity of CA IX by 22.6 %, 70.5 %, 58.8 % and 78 % respectively, as compared to the untreated EAC mice. Noticeably, mice received WEG-104-loaded niosomes (5 mg/kg/d) exhibited a significant decrease in CA IX activity relative to those received free-WEG-104 at the same dose ($p < 0.0001$) (Fig. 8A).

Similarly, the activity of CA XII was clearly inhibited by WEG-104 (5 and 10 mg/kg/d) in its free and loaded niosomal formulation (32 %, 65 %, 49 % and 78 %, respectively) in comparison to the untreated EAC mice. Interestingly, no apparent difference in CA IX and XII was noticed between free-WEG-104 at 10 mg/kg and WEG-104-loaded niosomes at 5 mg/kg (Fig. 8B).

3.7.4. Effect of WEG-104 on HIF-1 α and MMP-2

As represented in Figure 8C, a pronounced suppression of HIF-1 α was observed in EAC mice treated with either free-WEG-104 at 10 mg/kg/d or WEG-104-loaded niosomes at 5 and 10 mg/kg/d by 52 %, 44.5 % and 62 %, respectively, versus the untreated ones. Likewise, MMP-2 levels were obviously repressed in EAC mice treated with either free-WEG-104 at 5 and 10 mg/kg/d or WEG-104-loaded niosomes at 5 and

10 mg/kg/d by 25 %, 49 %, 42 % and 71 %, respectively, in comparison to the untreated ones (Fig. 8D).

3.7.5. Effect of WEG-104 on caspase-3

Defective apoptotic processes are associated with tumor cell growth and development. Among others, caspase-3 is implicated in cell survival and fate by regulating apoptosis (Vaeteewoottacharn et al., 2016). In this concern, EAC mice that received either 10 mg/kg/d of free-WEG-104 or 5 and 10 mg/kg/d of WEG-104-loaded niosomes revealed a prominent increase in caspase-3 by 3.2, 2.4, 4.2-fold versus the untreated ones. Administration of WEG-104-loaded niosomes (10 mg/kg/d) produced a noticeable increment in caspase-3 versus free-WEG-104 at the same dose ($p = 0.0147$) (Fig. 8E).

3.7.6. Effect of WEG-104 on VEGF immunoexpression

As shown in Fig. 9, VEGF was highly expressed in tumor tissues of EAC mice. Administration of 5 or 10 mg/kg of WEG-104 in its free or niosomal formulation for 20 d promoted a remarkable decrease in VEGF immunoreactive areas in tumor sections of EAC mice. Treatment of EAC mice with WEG-104-loaded niosomes at 5 or 10 mg/kg produced a pronounced decrease in VEGF immunoexpression compared to the corresponding free-WEG-104.

3.7.7. Histopathological results

Microscopic examination of stained EAC tumor sections revealed high tumor growth rate with large sized viable areas. Viable tumor areas are characterized by a marked degree of cellular anaplasia, pleomorphism, anisocytosis, nuclear dyschromasia, multiple atypical nuclei, numerous giant cells, and mitotic figures (Fig. 10a). In addition, sections of untreated EAC mice demonstrated minimal areas of necrosis. A slight

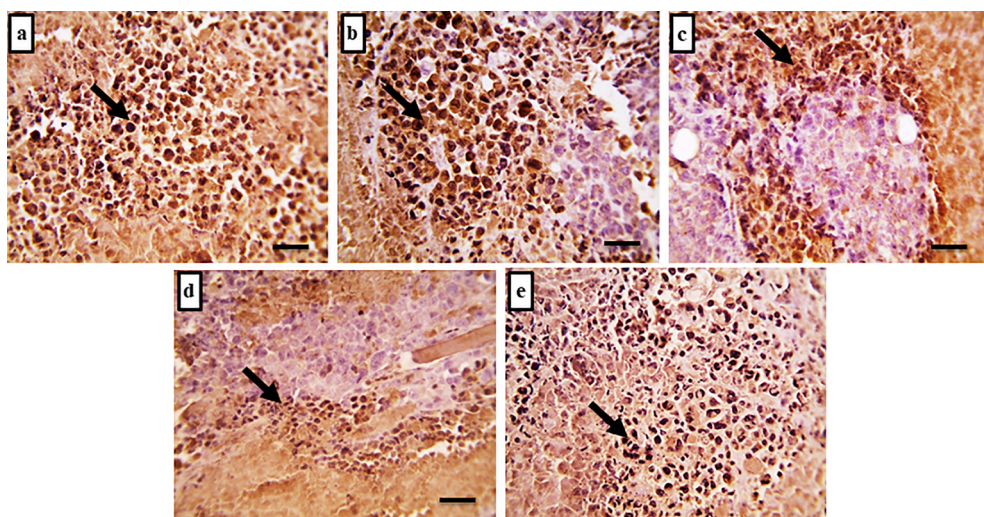


Fig. 9. Immunohistochemical investigation of VEGF in tumor tissues of EAC mice. (a) untreated EAC group, (b) free-WEG-104 (5 mg/kg) group, (c) free-WEG-104 (10 mg/kg) group, (d) WEG-104 niosomes (5 mg/kg) group, (e) WEG-104 niosomes (10 mg/kg) group, (f) percentage of VEGF immunoreactive area relative to total area through 6 fields *per* each section. Free and WEG-104 niosomes were intraperitoneally injected to EAC mice for 20 days using two doses (5 and 10 mg/kg/d). The black arrows indicate VEGF expression within tumor cells of EAC mice. Data were represented as mean \pm SD of 6 field. * *versus* untreated EAC, # *versus* free- WEG-104 (5 mg/kg/d), \$ *versus* free-WEG-104 (10 mg/kg/d).

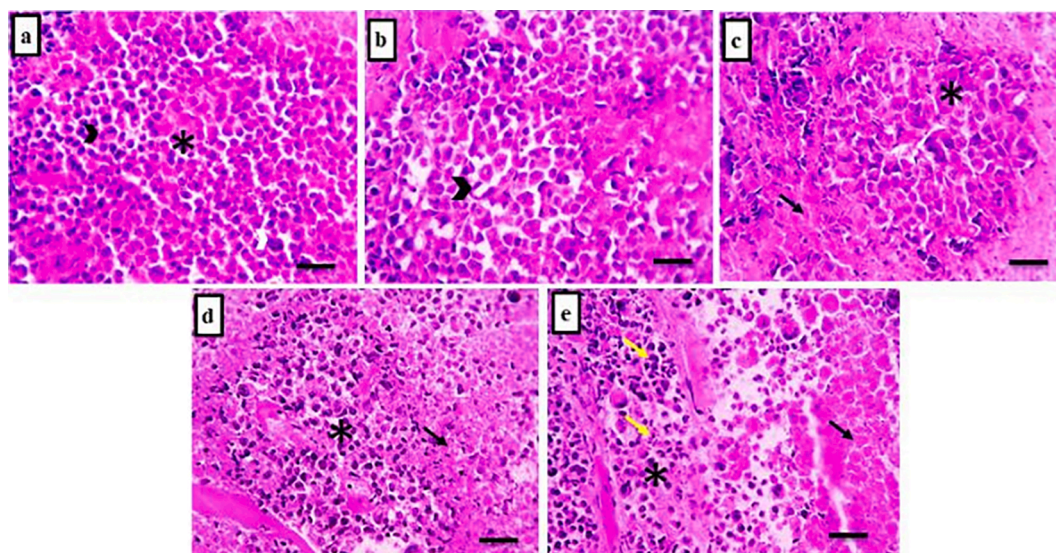
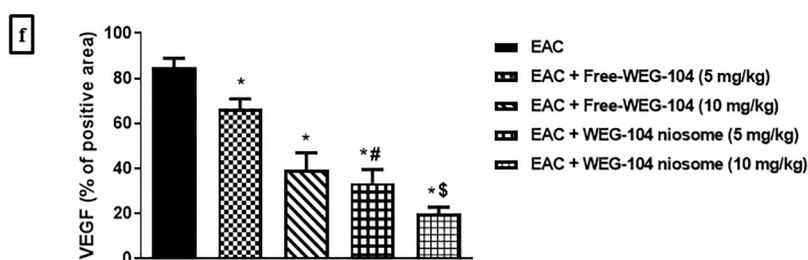


Fig. 10. Microscopic images of EAC solid tumor sections stained with H&E ($\times 400$, bar 50 μm). (a) section from untreated EAC group showing large viable areas (asterisk) with numerous giant cells (white arrowheads) and mitotic figures (black arrowhead), (b) section from EAC mice treated with free WEG-104 (5 mg/kg) showing a slight decrease in the size of viable areas, (c and d) sections from free WEG-104 (10 mg/kg) and WEG-104-loaded niosomes (5 mg/kg)-treated groups, respectively, showing a marked inhibition of tumor viable areas (asterisk) with an increased area of necrosis (black arrow), (e) section from WEG-104-loaded niosomes (10 mg/kg)-treated group showing wide areas of necrosis (black arrow) with a marked reduction in size of viable tumor areas (asterisk) and appearance of prominent nuclear pyknosis (yellow arrow). (For interpretation of the references to colour in this figure legend, the reader is referred to the web version of this article.)

inhibition of tumor viable areas was shown in tumor sections of EAC mice treated with free WEG-104 (5 mg/kg) (Fig. 10b), whereas free WEG-104 (10 mg/kg) and WEG-104-loaded niosomes (5 mg/kg) induced a marked inhibition of tumor viable areas. Regarding WEG-104-loaded niosomes (10 mg/kg)-treated EAC mice (Fig. 10c and d), wide areas of necrosis accompanied with a marked reduction in size and

number of viable tumor cells with prominent nuclear pyknosis were demonstrated (Fig. 10e).

3.7.8. Pharmacokinetic parameters and potential toxicity

Pharmacokinetic profile was assessed using both the Preadmet and the fu,p Predictor servers. Preadmet projected that compound WEG-104

possesses limited blood brain barrier penetration and that it only inhibits CYP 2C9, while not interacting with other CYP enzymes (**Supplementary Materials, Table S1**). In this setting, WEG-104 is not expected to result in neurotoxicity, and can be administered concurrently with other medications with low drug-drug interaction concerns. Furthermore, WEG-104 was found to be largely bound to plasma protein, with a lower quantity present as a free form, as anticipated by Preadmet and fu,p Predictor, respectively. Based on previous findings, WEG-104 should have a long half-life, allowing for less frequent dosage and improved patient compliance. WEG-104 was also evaluated for potential toxicity in various systems using the online server Toxpred. Results indicated that WEG-104 is considered safe with no potential carcinogenicity, mutagenicity, immunogenicity or hepatotoxicity (**Supplementary Materials, Table S2**).

4. Discussion

Targeting CA IX and XII is one of the cancer treatment strategies that has gained an increased interest recently due to their implication in tumor hypoxia, invasiveness, metastasis, and resistance to anticancer therapy (*Pastorekova and Gillies, 2019; Supuran, 2021*). Design and synthesis of selective inhibitors for human CA isoforms provide a promising approach for management of hypoxic solid tumors while minimizing side effects. In the current study, an isatin-bearing sulfonamide, WEG-104, was incorporated into a nanoparticulate delivery system (*i.e.*, niosomes), to allow for an enhanced and sustained anti-tumor activity *in vivo*. WEG-104-loaded niosomes of spherical morphologies displayed relatively high negative zeta potential (*i.e.*, -28.9 ± 0.8 mV) which indicates an adequate physical stability. The TEM image of WEG-104-loaded niosomes demonstrated monodispersed particles which is in agreement with the number-averaged diameter (red bars) that was assessed by dynamic light scattering. Intensity- and volume-averaged diameters (black and blue bars) highlighted the existence of few aggregates in the dispersion. Significant amount of the particles were in the range of 20–200 nm which might enhance accumulation within tumor tissues *via* enhanced permeability and retention effect. Although the developed niosomes were mainly comprised of non-ionic surfactants, negative zeta potential values were reported. This might be attributed to the ionization of free groups in the bilayer membrane, the orientation of hydroxyl groups towards water that results in alterations of ionic charges (*Gugleva et al., 2022*), and the presence of hydroxyl group in the cholesterol (*Eldehna et al., 2022; Kashef et al., 2020*). The nanosized niosomes resulted in *ca.* 93 % encapsulation of WEG-104, in agreement with previous studies which reported high encapsulation efficiency of niosomes developed utilizing Span® 60 (*Eldehna et al., 2022; Ghafelehbashhi et al., 2019; Kashef et al., 2020*). This might be attributed to the long saturated stearyl (C₁₈) chain length of Span® 60, its low HLB value (*i.e.*, 4.7) and high phase transition temperature (53 °C) which allows for the formation of less leaky niosomal vesicles (*i.e.*, of high entrapment efficiency). Presence of cholesterol in the niosomal composition allows for the formation of niosomes that possess a rigid membrane of lower fluidity, thus reducing drug leakage (*Ag Seleci et al., 2016; Li et al., 2022*). Moreover, the hydrophobic nature of WEG-104 might allow for its insertion into the bilayer of the niosomes enabling potential interactions (*e.g.*, hydrogen bonding, hydrophobic, *etc.*) between WEG-104 and the components of niosomes (*i.e.*, Span® 60, Tween® 40 and cholesterol), thus, enhancing entrapment efficiency. *In vitro* release studies revealed a sustained release profile for WEG-104-loaded niosomes as compared to the free drug. After 48 h, <50 % of the drug was released which might be attributed to the high entrapment of the drug in the lipophilic region (*i.e.*, bilayer membrane of the niosomes) (*Teaima et al., 2020*).

In this investigation, EAC cells were used for induction of subcutaneous solid tumor in female mice to study the anticancer activity of WEG-104. EAC mice model has been previously utilized to evaluate the antitumor effect of different cancer targeting agents (*Aziz et al., 2016;*

Mansour et al., 2022) and to study cancer-mediated diseases (*Mishra et al., 2018*). In the current study, WEG-104 displayed profound dose-dependent anticancer effect in EAC mice as confirmed by reduction of tumor volumes and weights, inhibition of tumor hypoxia and invasion markers thereby reducing the activity of CA IX, CA XII, HIF-1 α and MMP-2. In addition, WEG-104 decreased the expression of the angiogenesis factor (VEGF) in carcinoma tissues and promoted tumor cell apoptosis *via* activation of caspase-3. These events were accompanied with an increase in necrotic areas and a decrease in size of viable areas as demonstrated in the histopathological examination.

It has been suggested that CA IX and XII are overexpressed in many hypoxic solid tumors, and are associated with tumor oncogenic activity (*Abd-El Fattah et al., 2017*). Under hypoxic conditions, metabolic activity and oxygen consumption are increased by tumor tissues, leading to aberrant upregulation of HIF-1 α (*Chafe et al., 2021*). Among proteins targeted by HIF-1 α , CA IX and XII are involved in the regulation of tumor microenvironmental pH, favoring acidic extracellular milieu. Acidification of tumor extracellular environment plays a crucial role in tumor cell survival, progression, invasion and metastasis, and contributes to cancer chemotherapy resistance (*Abd-El Fattah et al., 2017; Parkkila et al., 2000*). Thus, inhibition of CA IX and XII by WEG-104, for example, could impede the tumor progression in EAC mice.

Anomalous angiogenesis is a key process for tumor proliferation and metastasis which involves the induction of proangiogenic factors including VEGF (*Ebos et al., 2002*). In this regard, WEG-104 attenuated VEGF expression in the tumor tissues of EAC, probably by inhibiting the activity of CA IX and XII. Silencing CA IX isoenzyme reduced angiogenesis and induced profound cell death in pulmonary microvascular endothelial cell culture thereby attenuating acidosis (*Lee et al., 2018*). In a previous study, inhibition of CA IX and CA XII by acetazolamide, an inhibitor of hypoxia-inducible carbonic anhydrase, potentiated the antiangiogenic effect of bevacizumab, leading to amelioration of the hypoxic adaptation and stronger reduction of tumor proliferation in a mouse model of cholangiocarcinoma (*Vaeteewoottacharn et al., 2016*).

Matrix metalloproteinases (MMPs) are zinc-dependent endopeptidases associated with disruption of extracellular matrix, thus contributing to invasion of solid tumors (*Alaseem et al., 2019*). In a study conducted by *Horie et al.*, treatment of human umbilical vein endothelial cell culture with exosomes overexpressing CA XII induced MMP-2 upregulation, promoted cell migration, tube formation and angiogenesis (*Horie et al., 2017*). In this study, WEG-104 reduced the level of MMP-2, a member of MMPs, in tumor tissues of EAC mice. The current results are in agreement with an earlier study in which knocking out CA XII suppressed MMP-2 levels, and resulted in halting the migration and invasiveness of breast cancer cells (*Hsieh et al., 2010*).

In the present investigation, WEG-104 incited the tumor cell regression and death thereby triggering the apoptotic factor, caspase-3, in EAC mice. In agreement, a previous study has demonstrated that acetazolamide, a CA inhibitor, enhanced caspase-3 *via* activating the intrinsic pathway of apoptosis in isolated tumor tissues of EAC (*Abd-El Fattah et al., 2017*). Intracellular acidification caused by CA IX inhibition may lead to production of cytoplasmic ceramides which play a key role in regulating caspase-3, cell fate, and apoptosis in human cancer cells (*Cianchi et al., 2010*).

Administration of WEG-104-loaded niosomes at a dose of 5 mg/kg showed similar efficacy to the free drug at a higher dose (*i.e.*, 10 mg/kg). WEG-104-loaded niosomes at a dose of 10 mg/kg exhibited superior antitumor activity evidenced by reduced tumor weight and volume, marked reduction in the activity of CA IX and XII, and suppression of HIF-1 α and MMP-2. Moreover, a prominent increase of caspase 3, and pronounced decrease in VEGF immune expression were also observed in the treated animals. This might be attributed to the prolonged circulation of the drug loaded-nanovesicles and enhanced accumulation within tumor tissues *via* enhanced permeability and retention, compared to the free drug (*Elsababy and Wooley, 2012*).

5. Conclusion

WEG-104, a newly synthesized CA IX and CA XII inhibitor, was synthesized and evaluated for its antitumor activity. WEG-104, exhibited a profound antitumor activity in a model of EAC solid tumor *via* inhibition of hypoxia-mediated tumor cell survival and migration. Incorporation of WEG-104 into niosomes displayed an enhanced antitumor activity evidenced by reduced tumor weight and volume, marked reduction in the activity of CA IX and XII, and suppression of HIF-1 α and MMP-2. Prolonged circulation of the drug loaded into the nanovesicles and enhanced accumulation within tumor tissues *via* enhanced permeability and retention might explain the superior antitumor activity of the drug-loaded niosomes compared to the free drug. Future work will include further mechanistic studies to elucidate the antitumor effect of WEG-104 in other models of hypoxic solid tumors.

Funding

The authors acknowledge financial support from the Researchers Supporting Project number (RSP-2021/103), King Saud University, Riyadh, Saudi Arabia.

CRedit authorship contribution statement

Wagdy M. Eldehna: Conceptualization, Methodology, Supervision, Writing – review & editing. **Mahmoud A. El Hassab:** Methodology, Formal analysis. **Nahla A. Abdelshafi:** Methodology, Formal analysis, Writing – original draft. **Rana A. Eissa:** Methodology, Formal analysis. **Nadeen H. Diab:** Methodology. **Ekram H. Mohamed:** Methodology, Formal analysis, Writing – original draft. **Mamdouh A. Oraby:** Methodology, Formal analysis, Writing – original draft. **Sara T. Al-Rashood:** Supervision. **Rana G. Eissa:** Methodology, Formal analysis, Writing – original draft. **Zainab M. Elsayed:** Methodology. **Alessio Nocentini:** Methodology. **Claudio T. Supuran:** Conceptualization, Supervision. **Mahmoud Elsbahy:** Conceptualization, Methodology, Supervision, Writing – original draft, Writing – review & editing. **Noura G. Eissa:** Methodology, Formal analysis, Writing – original draft, Writing – review & editing.

Declaration of Competing Interest

The authors declare that they have no known competing financial interests or personal relationships that could have appeared to influence the work reported in this paper.

Data availability

Data will be made available on request.

Appendix A. Supplementary material

Supplementary data to this article can be found online at <https://doi.org/10.1016/j.ijpharm.2022.122537>.

References

- Abd-El Fattah, A.A., Darwish, H.A., Fathy, N., Shouman, S.A., 2017. Carbonic anhydrase inhibition boosts the antitumor effects of Imatinib mesylate *via* potentiating the antiangiogenic and antimetastatic machineries. *Toxicol. Appl. Pharmacol.* 316, 123–138. <https://doi.org/10.1016/j.taap.2016.12.017>.
- Abdel-Aziz, H.A., Eldehna, W.M., Keeton, A.B., Piazza, G.A., Kadi, A.A., Attwa, M.W., Abdelhameed, A.S., Attia, M.I., 2017. Isatin-benzozazine molecular hybrids as potential antiproliferative agents: synthesis and *in vitro* pharmacological profiling. *Drug Des. Devel. Ther.* 11, 2333–2346. <https://doi.org/10.2147/DDDT.S140164>.
- Ag Seleci, D., Seleci, M., Walter, J.G., Stahl, F., Schepel, T., 2016. Niosomes as nanoparticulate drug carriers: fundamentals and recent applications. *J. Nanomater.* 2016 <https://doi.org/10.1155/2016/7372306>.

- Alaseem, A., Alhazzani, K., Dondapati, P., Alobod, S., Bishayee, A., Rathinavelu, A., 2019. Matrix Metalloproteinases: a challenging paradigm of cancer management. *Semin. Cancer Biol.* 56, 100–115. <https://doi.org/10.1016/j.semcancer.2017.11.008>.
- Allam, A., El-Mokhtar, M.A., Elsbahy, M., 2019. Vancomycin-loaded niosomes integrated within pH-sensitive *in-situ* forming gel for treatment of ocular infections while minimizing drug irritation. *J. Pharm. Pharmacol.* 71, 1209–1221. <https://doi.org/10.1111/jphp.13106>.
- Allam, A., Elsbahy, M., El Badry, M., Eleraky, N.E., 2021. Betaxolol-loaded niosomes integrated within pH-sensitive *in situ* forming gel for management of glaucoma. *Int. J. Pharm.* 598 <https://doi.org/10.1016/j.ijpharm.2021.120380>.
- Aparajay, P., Dev, A., 2022. Functionalized niosomes as a smart delivery device in cancer and fungal infection. *Eur. J. Pharm. Sci.* 168, 106052 <https://doi.org/10.1016/j.ejps.2021.106052>.
- Aziz, M.A., Serya, R.A.T., Lasheen, D.S., Abdel-Aziz, A.K., Esmat, A., Mansour, A.M., Singab, A.N.B., Abouzid, K.A.M., 2016. Discovery of potent VEGFR-2 inhibitors based on Fluoropyrimidine and Thienopyrimidine Scaffolds as cancer targeting agents. *Sci. Rep.* 6, 1–20. <https://doi.org/10.1038/srep24460>.
- Bray, F., Ferlay, J., Soerjomataram, I., Siegel, R.L., Torre, L.A., Jemal, A., 2018. Global cancer statistics 2018: GLOBOCAN estimates of incidence and mortality worldwide for 36 cancers in 185 countries. *CA Cancer J. Clin.* 68, 394–424. <https://doi.org/10.3322/caac.21492>.
- Chafe, S.C., Vizeacoumar, F.S., Venkateswaran, G., Nemirovsky, O., Awrey, S., Brown, W. S., McDonald, P.C., Carta, F., Metcalfe, A., Karasinska, J.M., Huang, L., Muthuswamy, S.K., Schaeffer, D.F., Renouf, D.J., Supuran, C.T., Vizeacoumar, F.J., Dedhar, S., 2021. Genome-wide synthetic lethal screen unveils novel CAIX-NFS1/xCT axis as a targetable vulnerability in hypoxic solid tumors. *Sci. Adv.* 7, 1–16. <https://doi.org/10.1126/sciadv.abj0364>.
- Cianchi, F., Vinci, M.C., Supuran, C.T., Peruzzi, B., De Giuli, P., Fasolis, G., Perigli, G., Pastorekova, S., Papucci, L., Pini, A., Masini, E., Puccetti, L., 2010. Selective inhibition of carbonic anhydrase IX decreases cell proliferation and induces ceramide-mediated apoptosis in human cancer cells. *J. Pharmacol. Exper. Therap.* 334, 710–719. <https://doi.org/10.1124/jpet.110.167270>.
- Ebos, J.M.L., Tran, J., Master, Z., Dumont, D., Melo, J.V., Buchdunger, E., Kerbel, R.S., 2002. Imatinib mesylate (STI-571) reduces Bcr-Abl-mediated vascular endothelial growth factor secretion in chronic myelogenous leukemia. *Mol. Cancer Res. : MCR* 1, 89–95.
- Eldehna, W.M., Al-Ansary, G.H., Bua, S., Nocentini, A., Gratteri, P., Altoukhy, A., Ghabbour, H., Ahmed, H.Y., Supuran, C.T., 2017. Novel indolin-2-one-based sulfonamides as carbonic anhydrase inhibitors: synthesis, *in vitro* biological evaluation against carbonic anhydrases isoforms I, II, IV and VII and molecular docking studies. *Eur. J. Med. Chem.* 127, 521–530. <https://doi.org/10.1016/j.ejmech.2017.01.017>.
- Eldehna, W.M., Nocentini, A., Al-Rashood, S.T., Hassan, G.S., Alkahtani, H.M., Almezhia, A.A., Reda, A.M., Abdel-Aziz, H.A., Supuran, C.T., 2018. Tumor-associated carbonic anhydrase isoform IX and XII inhibitory properties of certain isatin-bearing sulfonamides endowed with *in vitro* antitumor activity towards colon cancer. *Bioorg. Chem.* 81, 425–432. <https://doi.org/10.1016/j.bioorg.2018.09.007>.
- Eldehna, W.M., Al-Rashood, S.T., Al-Warhi, T., Eskandrani, R.O., Alharbi, A., El Kerdawy, A.M., 2021. Novel oxindole/benzofuran hybrids as potential dual CDK2/GSK-3 β inhibitors targeting breast cancer: design, synthesis, biological evaluation, and *in silico* studies. *J. Enzyme Inhib. Med. Chem.* 36, 270–285. <https://doi.org/10.1080/14756366.2020.1862101>.
- Eldehna, W.M., El Hassab, M.A., Abdelshafi, N.A., Al-Zahraa Sayed, F., Fares, M., Al-Rashood, S.T., Elsayed, Z.M., Abdel-Aziz, M.M., Elkhaed, E.B., Elsbahy, M., Eissa, N. G., 2022. Development of potent nanosized isatin-isonicotinohydrazide hybrid for management of Mycobacterium tuberculosis. *Int. J. Pharm.* 612, 121369 <https://doi.org/10.1016/j.ijpharm.2021.121369>.
- Elsbahy, M., Wooley, K.L., 2012. Design of polymeric nanoparticles for biomedical delivery applications. *Chem. Soc. Rev.* 41, 2545–2561. <https://doi.org/10.1039/c2cs15260f>.
- Gao, S., Zang, J., Gao, Q., Liang, X., Ding, Q., Li, X., Xu, W., Chou, C.J., Zhang, Y., 2017. Design, synthesis and anti-tumor activity study of novel histone deacetylase inhibitors containing isatin-based caps and o-phenylenediamine-based zinc binding groups. *Bioorg. Med. Chem.* 25, 2981–2994. <https://doi.org/10.1016/j.bmc.2017.03.036>.
- Ge, X., Wei, M., He, S., Yuan, W.E., 2019. Advances of non-ionic surfactant vesicles (niosomes) and their application in drug delivery. *Pharmaceutics* 11. <https://doi.org/10.3390/pharmaceutics11020055>.
- Ghafahebashi, R., Akbarzadeh, I., Tavakkoli Yaraki, M., Lajevardi, A., Fatemizadeh, M., Heidarpour Saremi, L., 2019. Preparation, physicochemical properties, *in vitro* evaluation and release behavior of cephalixin-loaded niosomes. *Int. J. Pharm.* 569, 118580 <https://doi.org/10.1016/j.ijpharm.2019.118580>.
- Goodman, V.L., Rock, E.P., Dagher, R., Ramchandani, R.P., Abraham, S., Gobburu, J.V. S., Booth, B.P., Verbois, S.L., Morse, D.E., Liang, C.Y., Chidambaram, N., Jiang, J.X., Tang, S., Mahjoob, K., Justice, R., Pazdur, R., 2007. Approval summary: Sunitinib for the treatment of imatinib refractory or intolerant gastrointestinal stromal tumors and advanced renal cell carcinoma. *Clin. Cancer Res.* 13, 1367–1373. <https://doi.org/10.1158/1078-0432.CCR-06-2328>.
- Gugleva, V., Michailova, V., Mihaylova, R., Momekov, G., Zaharieva, M.M., Najdenski, H., Petrov, P., Rangelov, S., Forsy, A., Trzebiecka, B., Momekova, D., 2022. Formulation and evaluation of hybrid niosomal *in situ* gel for intravesical co-delivery of curcumin and gentamicin sulfate. *Pharmaceutics* 14. <https://doi.org/10.3390/pharmaceutics14040747>.
- Horie, K., Kawakami, K., Fujita, Y., Sugaya, M., Kameyama, K., Mizutani, K., Deguchi, T., Ito, M., 2017. Exosomes expressing carbonic anhydrase 9 promote angiogenesis.

- Biochem. Biophys. Res. Commun. 492, 356–361. <https://doi.org/10.1016/j.bbrc.2017.08.107>.
- Hsieh, M.-J., Chen, K.-S., Chiou, H.-L., Hsieh, Y.-S., 2010. Carbonic anhydrase XII promotes invasion and migration ability of MDA-MB-231 breast cancer cells through the p38 MAPK signaling pathway. *Eur. J. Cell Biol.* 89, 598–606. <https://doi.org/10.1016/j.ejcb.2010.03.004>.
- Ibrahim, H.S., Abou-Seri, S.M., Tanc, M., Elaasser, M.M., Abdel-Aziz, H.A., Supuran, C.T., 2015. Isatin-pyrazole benzenesulfonamide hybrids potently inhibit tumor-associated carbonic anhydrase isoforms IX and XII. *Eur. J. Med. Chem.* 103, 583–593. <https://doi.org/10.1016/j.ejmech.2015.09.021>.
- Kashef, M.T., Saleh, N.M., Assar, N.H., Ramadan, M.A., 2020. The antimicrobial activity of ciprofloxacin-loaded niosomes against ciprofloxacin-resistant and biofilm-forming *Staphylococcus aureus*. *Infect. Drug Resist.* 13, 1619–1629.
- Lee, J.Y., Alexeyev, M., Kozhukhar, N., Pastukh, V., White, R., Stevens, T., 2018. Carbonic anhydrase IX is a critical determinant of pulmonary microvascular endothelial cell pH regulation and angiogenesis during acidosis. *Am. J. Physiol. Lung Cell. Mol. Physiol.* 315, L41–L51. <https://doi.org/10.1152/ajplung.00446.2017>.
- Li, D., Martini, N., Wu, Z., Chen, S., Falconer, J.R., Locke, M., Zhang, Z., Wen, J., 2022. Niosomal nanocarriers for enhanced dermal delivery of epigallocatechin gallate for protection against oxidative stress of the skin. *Pharmaceutics* 14. <https://doi.org/10.3390/pharmaceutics14040726>.
- Li, W., Zhao, S.J., Gao, F., Lv, Z.S., Tu, J.Y., Xu, Z., 2018. Synthesis and in vitro anti-tumor, anti-mycobacterial and anti-HIV Activities of diethylene-glycol-tethered bis-isatin derivatives. *ChemistrySelect* 3, 10250–10254. <https://doi.org/10.1002/slct.201802185>.
- Liu, Y., Jiang, Y., Zhang, M., Tang, Z., He, M., Bu, W., 2018. Modulating hypoxia via nanomaterials chemistry for efficient treatment of solid tumors. *Acc. Chem. Res.* 51, 2502–2511. <https://doi.org/10.1021/acs.accounts.8b00214>.
- Lorke, D., 1983. A new approach to practical acute toxicity testing. *Arch. Toxicol.* 54, 275–287. <https://doi.org/10.1007/BF01234480>.
- Mansour, M.A., Oraby, M.A., Muhammad, Z.A., Lasheen, D.S., Gaber, H.M., Abouzid, K. A.M., 2022. Identification of novel furo[2,3-d]pyrimidine based chalcones as potent anti-breast cancer agents: synthesis, in vitro and in vivo biological evaluation. *RSC Adv.* 12, 8193–8201. <https://doi.org/10.1039/d2ra00889k>.
- McCormack, P.L., 2015. Nintedanib: first global approval. *Drugs* 75, 129–139. <https://doi.org/10.1007/s40265-014-0335-0>.
- Mishra, S., Tamta, A.K., Sarikhani, M., Desingu, P.A., Kizkekra, S.M., Pandit, A.S., Kumar, S., Khan, D., Raghavan, S.C., Sundaresan, N.R., 2018. Subcutaneous Ehrlich Ascites Carcinoma mice model for studying cancer-induced cardiomyopathy. *Sci. Rep.* 8, 5599. <https://doi.org/10.1038/s41598-018-23669-9>.
- Mohamed, H.B., El-Shanawany, S.M., Hamad, M.A., Elsabahy, M., 2017. Niosomes: a strategy toward prevention of clinically significant drug incompatibilities. *Sci. Rep.* 7, 1–14. <https://doi.org/10.1038/s41598-017-06955-w>.
- Mosmann, T., 1983. Rapid colorimetric assay for cellular growth and survival: Application to proliferation and cytotoxicity assays. *J. Immunol. Methods* 65, 55–63. [https://doi.org/10.1016/0022-1759\(83\)90303-4](https://doi.org/10.1016/0022-1759(83)90303-4).
- Parkkila, S., Rajaniemi, H., Parkkila, A.K., Kivelä, J., Waheed, A., Pastoreková, S., Pastorek, J., Sly, W.S., 2000. Carbonic anhydrase inhibitor suppresses invasion of renal cancer cells in vitro. *Proceedings of the National Academy of Sciences of the United States of America* 97, 2220–2224. <https://doi.org/10.1073/pnas.040554897>.
- Pastorekova, S., Gillies, R.J., 2019. The role of carbonic anhydrase IX in cancer development: links to hypoxia, acidosis, and beyond. *Cancer Metastasis Rev.* 38, 65–77. <https://doi.org/10.1007/s10555-019-09799-0>.
- Ramadan, A.A., Eladawy, S.A., El-Enin, A.S.M.A., Hussein, Z.M., 2020. Development and investigation of timolol maleate niosomal formulations for the treatment of glaucoma. *J. Pharm. Investig.* 50, 59–70. <https://doi.org/10.1007/s40005-019-00427-1>.
- Saafan, H.A., Ibrahim, K.M., Thabet, Y., Elbeltagy, S.M., Eissa, R.A., Ghaleb, A.H., Ibrahim, F., Elsabahy, M., Eissa, N.G., 2021. Intratracheal administration of chloroquine-loaded niosomes minimize systemic drug exposure. *Pharmaceutics* 13, 1677.
- Supuran, C.T., 2008. Carbonic anhydrases: Novel therapeutic applications for inhibitors and activators. *Nat. Rev. Drug Discov.* 7, 168–181. <https://doi.org/10.1038/nrd2467>.
- Supuran, C.T., 2020. Experimental carbonic anhydrase inhibitors for the treatment of hypoxic tumors. *J. Exp. Pharmacol.* 12, 603–617. <https://doi.org/10.2147/JEP.S265620>.
- Supuran, C.T., 2021. Carbonic anhydrase inhibitors: an update on experimental agents for the treatment and imaging of hypoxic tumors. *Expert Opin. Invest. Drugs* 30, 1197–1208. <https://doi.org/10.1080/13543784.2021.2014813>.
- Teaima, M.H., El Mohamady, A.M., El-Nabarawi, M.A., Mohamed, A.I., 2020. Formulation and evaluation of niosomal vesicles containing ondansetron HCL for trans-mucosal nasal drug delivery. *Drug Dev. Ind. Pharm.* 46, 751–761. <https://doi.org/10.1080/03639045.2020.1753061>.
- Thabet, Y., Elsabahy, M., Eissa, N.G., 2021. Methods for preparation of niosomes: a focus on thin-film hydration method. *Methods* 1–7. <https://doi.org/10.1016/j.ymeth.2021.05.004>.
- Trott, O., Olson, A.J., 2010. AutoDock Vina: improving the speed and accuracy of docking with a new scoring function, efficient optimization, and multithreading. *J. Comput. Chem.* 31, 455–461. <https://doi.org/10.1002/jcc.21334>.
- Vaeteewoottacharn, K., Kariya, R., Dana, P., Fujikawa, S., Matsuda, K., Ohkuma, K., Kudo, E., Kraiklang, R., Wongkham, C., Wongkham, S., Okada, S., 2016. Inhibition of carbonic anhydrase potentiates bevacizumab treatment in cholangiocarcinoma. *Tumour Biol. : J. Int. Soc. Oncodevelop. Biol. Med.* 37, 9023–9035. <https://doi.org/10.1007/s13277-016-4785-8>.
- Vats, L., Kumar, R., Bua, S., Nocentini, A., Gratteri, P., Supuran, C.T., Sharma, P.K., 2019. Continued exploration and tail approach synthesis of benzenesulfonamides containing triazole and dual triazole moieties as carbonic anhydrase I, II, IV and IX inhibitors. *Eur. J. Med. Chem.* 183, 111698. <https://doi.org/10.1016/j.ejmech.2019.111698>.